TO APPEAR IN THE ASTROPHYSICAL JOURNAL
Preprint typeset using LATEX style emulateapj v. 10/09/06

arXiv:astro-ph/0603351v2 27 Mar 2007

THERMAL STABILITY OF WHITE DWARFS ACCRETING HYDROGEN-RICH MATTER AND PROGENITORS OF TYPE IA SUPERNOVAE

KEN'ICHI NOMOTO
Department of Astronomy, Graduate School of Science, University of Tokyo, 7-3-1 Hongo, Bunkyo-ku, Tokyo 113-0033, Japan

HIDEYUKI SAIO
Astronomical Institute, Graduate School of Science, Tohoku University, Sendai, 980-8578, Japan

MARIKO KATO
Department of Astronomy, Keio University, Hiyoshi, Kouhoku-ku, Yokohama 223-8521, Japan

AND

IZUMI HACHISU
Department of Earth Science and Astronomy, College of Arts and Sciences, University of Tokyo, Komaba, Meguro-ku, Tokyo 153-8902, Japan

to appear in the Astrophysical Journal

ABSTRACT

We revisit the properties of white dwarfs accreting hydrogen-rich matter by constructing steady-state models, in which hydrogen shell burning consumes hydrogen at the same rate as the white dwarf accretes it. We obtain such steady-state models for various accretion rates and white dwarf masses. We confirm that these steady models are thermally stable only when the accretion rate is higher than $\sim 10^{-7} M_\odot$ yr^{-1}. We show that recent models of "quiescent burning" in the "surface hydrogen burning" at a much wider range of accretion rates results from the too large zone mass in the outer part of the models; hydrogen burning must occur in a much thinner layer. A comparison of the positions on the HR diagram suggests that most of the luminous supersoft X-ray sources are white dwarfs accreting matter at rates high enough that the hydrogen burning shell is thermally stable. Implications on the progenitors of Type Ia supernovae are discussed.

Subject headings: accretion – binaries: close – stars: evolution – novae, cataclysmic variables — supernovae: general – white dwarfs

1. INTRODUCTION

It is widely accepted that progenitors of Type Ia supernovae (SNe Ia) are mass accreting C-O white dwarfs, although the nature of the progenitor binary systems is still under debate (e.g., Nomoto et al. 1997; Hillebrandt & Niemeyer 2000; Nomoto et al. 2003). In the most popular model, the Chandrasekhar mass model, a C-O white dwarf accretes mass until it grows in mass to $M = 1.38\ M_\odot$, then explodes as an SN Ia (e.g., Nomoto 1982; Nomoto et al. 1984; Livio 2000). To find a path to SNe Ia is to find a way for a C-O white dwarf to increase its central density and temperature to carbon ignition as the Chandrasekhar limit is approached. If the mass donor is a normal star, the stability of the hydrogen burning shell in the accreting white dwarf is crucial for its evolution.

A hydrogen-shell burning is ignited in an accreting white dwarf when a certain amount of hydrogen-rich matter is accumulated in the envelope. The shell burning is unstable to flash if the accretion rate is lower than a critical rate (e.g., Sugimoto & Miyaji 1981). The flash is stronger if the white dwarf is cooler and the accretion is slower (Paczyński & Żytkow 1978; Sion et al. 1979; Fujimoto 1982a,b). If the shell flash is strong enough to trigger a nova outburst, most part of the envelope would be lost from the system. Moreover, a part of the original white dwarf matter could be dredged up and lost in the outburst wind. Therefore, the white dwarf mass could decrease after one cycle of nova outburst (e.g., Prialnik 1986; Prialnik & Kovetz 1995; Yaron et al. 2005), although Townsley & Bildsten (2004) did not find such indication in the nova systems.

If the accretion rate $\dot{M}$ is high enough, on the other hand, the shell burning is stable and the mass of the white dwarf increases with accretion. Thus, the critical accretion rate $\dot{M}_{\rm stable}$, above which hydrogen shell burning is stable, is an important physical value for the evolution of accreting white dwarfs. (For $\dot{M}$ being appreciably higher than $\dot{M}_{\rm stable}$, see §5).

Studies on the thermal instability of a thin nuclear-burning shell began when Schwarzschild & Härm (1965) found that helium shell flashes were caused by a thermal instability of a shell around a C-O core of an evolved star. Since then, the stability of a nuclear shell burning in an accreting white dwarf has been extensively studied in connection with nova outbursts (e.g., Sugimoto & Fujimoto 1978, and references therein). Sienkiewicz (1980) obtained the stability boundary by examining thermal stability of steady-state models for accreting white dwarfs of various masses. The stability boundary, which is $\dot{M}_{\rm stable} \simeq 10^{-7} M_\odot {\rm yr}^{-1}$ at $M = 0.8 M_\odot$ and higher for more massive white dwarfs, is consistent with fully time-dependent calculations (e.g., Paczyński & Żytkow 1978; Sion et al. 1979; Iben 1982; Prialnik & Kovetz 1995; Yaron et al. 2005).

Recently, Starrfield et al. (2004) published new models of accreting white dwarfs called "surface hydrogen burning" models. They tried to show that if a very hot white dwarf

Electronic address: nomoto@astron.s.u-tokyo.ac.jp
Electronic address: saio@astr.tohoku.ac.jp
Electronic address: mariko@educ.cc.keio.ac.jp
Electronic address: hachisu@chianti.c.u-tokyo.ac.jp

after a nova outburst started accreting hydrogen-rich matter, it developed surface hydrogen burning that stably converts hydrogen into helium and helium into heavier elements; then the white dwarf mass could grow to the Chandrasekhar limit. They obtained such "surface hydrogen burning" models for accretion rates ranging from 1.6×10^{-9} to $8.0 \times 10^{-7} M_\odot$ yr^{-1}, and identified these models as supersoft X-ray sources. The properties of their models, however, clearly contradict previous results of evolutionary and steady-state models (e.g., Iben 1982; Prialnik & Kovetz 1995; Sienkiewicz 1980).

We will show in this paper that the contrasting properties of the "surface hydrogen burning" models result from too coarse zoning for the envelope structure. We first recalculate steady-state models for various accretion rates and white dwarf masses. If accretion continues long enough, the mean luminosity of the white dwarf should approach the steady-state luminosity irrespective of the initial luminosity. We then examine the thermal stability of these models to confirm the results of Sienkiewicz (1980) using the updated input physics.

In obtaining our steady models, we solve the full stellar structure in order to avoid the approximations made in the one zone models (Fujimoto 1982a). We present more detailed numerical models, their stabilities, and the exact stability boundary values in tabular forms and formula for a wider range of the white dwarf mass and the accretion rate compared with Sienkiewicz (1975, 1980).

We have adopted linear stability analysis mainly because we can avoid long evolution calculations for many models. In oder to judge the stability by evolution calculations as in Iben (1982), we have to adopt sufficiently short time steps, which demands long cpu times. Also, by a linear analysis we can determine the stability boundary exactly, while it is difficult for the evolutionary calculations, because near the stability boundary the growth time is so long that it would be difficult to distinguish the variation due to thermal instability from a normal evolutionary change.

Then we examine the "surface hydrogen burning" models by Starrfield et al. (2004) and discuss the reason for the discrepancy with the previous results. Our numerical methods are described in §2 and our results are given in §3. In §4 we discuss the reason for the discrepancy between Starrfield et al.'s (2004) models and the previous results, and compare the loci on the HR diagram of our steady-state models to those of luminous supersoft X-ray sources. Implications on the progenitors of Type Ia supernovae are discussed in §5.

2. STEADY-STATE MODELS

We have constructed steady-state models for white dwarfs accreting matter of solar composition. The steady-state model consists of a C-O core surrounded by a hydrogen-rich envelope of the solar abundances. At the bottom of the envelope, hydrogen is burned at the same rate as the star accretes it; i.e.,

$$L_{\rm n} = XQ\dot{M}, \tag{1}$$

where $L_{\rm n}$ is the luminosity due to hydrogen burning, X is the hydrogen mass fraction in the accreted matter, $Q = 6.4 \times 10^{18}$erg g^{-1} energy generated when 1 gram of hydrogen is converted to helium, and $\dot{M}$ is the mass accretion rate. The nuclear reaction rates are taken from Caughlan & Fowler (1988) with the weak and intermediate screening factors by Graboske et al. (1973). The helium layer and helium shell burning are neglected for simplicity, because the stability of hydrogen burning in a thin shell is mainly determined by the structure of hydrogen-rich layer above the hydrogen burning-shell (Sugimoto & Fujimoto 1978). Also the helium layer is thin and the energy release is only 10 % of hydrogen burning so that the effects on the stability of hydrogen burning shell are negligible (see Paczyński (1983) for the study of the effect of heat flux from the core). The compressional heating due to accretion is included in the same way as in Kawai et al. (1987); i.e., the heating rate per unit mass, $\epsilon_{\rm g}$, is given by

$$\epsilon_{\rm g} = \frac{\dot{M}}{M} T \frac{ds}{d\ln q}, \tag{2}$$

where s is the entropy per unit mass, and $q \equiv M_r/M$ with M_r being the mass included in the sphere of radius r. The chemical composition of the C-O core is adopted as $(X_{\rm C}, X_{\rm O}, X_{\rm Z}) = (0.48, 0.50, 0.02)$ where $X_{\rm Z}$ denotes the mass fraction of heavy elements scaled by the solar composition. Opacity is obtained from OPAL opacity tables (Iglesias & Rogers 1996).

Tables 1 - 4 summarize the properties of several steady state models for given M and $\dot{M}$: the mass of the H-rich envelope $\Delta M_{\rm env}$, $r_{\rm H}$, $T_{\rm H}$, $\rho_{\rm H}$, $P_{\rm H}$, and $\epsilon_{\rm n}$ at the bottom of the H-rich envelope, and $L_{\rm n}$, L, R, and $T_{\rm eff}$ at the surface.

3. THERMAL STABILITY OF MODELS

For each steady-state model, we have examined the thermal stability against a linear perturbation. Assuming that perturbations to stellar structure occur without disturbing hydrostatic balance and that they are spherically symmetric, we have examined thermal stability by slightly modifying the Henyey-type relaxation code that we use to compute stellar structure. As well known, in the Henyey relaxation, a correction δy_i $(i = 1, 2, 3, 4)$ to a variable y_i is obtained by solving inhomogeneous linear equations expressed as

$$\mathcal{H}\delta y = D \tag{3}$$

where $\boldsymbol{\mathcal{H}}$ is a $4N \times 4N$ matrix with N being the number of mesh points, δy a vector consists of δy_i at each mesh point, and D is a vector with $4N$ components representing the deviation of the variables y_i from the correct values. In thermal stability analysis for a stellar model, we regard δy_i as a perturbation to the variable y_i which satisfies the differential equations for stellar structure so that the inhomogeneous terms diminish; i.e., $D = 0$. We express the temporal variation of perturbed quantities by $\exp(\sigma t)$ so that we replace the time derivative of entropy $\partial \delta s / \partial t$ with $\sigma \delta s$.

We write the modified Henyey matrix as $\overline{\mathcal{H}}$. Then, we obtain homogeneous equations

$$\overline{\mathcal{H}}\delta y = 0, \tag{4}$$

which govern the perturbation and an eigenvalue σ.

The eigenvalue σ is obtained by searching for a value which makes the matrix $\overline{\mathcal{H}}$ singular. If there is a positive σ, the structure is thermally unstable with a growth rate of $\tau_{\rm g} = 1/\sigma$. If all the eigenvalues are negative, on the other hand, we judge that the stellar model is thermally stable. The obtained $\tau_{\rm g}$ and the stability for several models are summarized in Tables 1 - 4.

Figure 1 shows the steady-state models in the HR diagram computed for C-O white dwarfs of $M = 0.5 - 1.38 M_\odot$ which accrete hydrogen-rich matter at various rates $\dot{M}$. The lowest luminosity in Figure 1 corresponds to $\dot{M} = 10^{-10} M_\odot$ yr^{-1}.

As $\dot{M}$ gets larger along a sequence of models with given mass M, the luminosity asymptotically approaches a limiting value of $L_{\rm RG}$, which corresponds to the red-giant luminosity determined by the "core mass - luminosity" relation

TABLE 1
STEADY HYDROGEN BURNING MODELS ($M = 1.35 M_\odot$)

$\dot{M}(M_\odot \mathrm{yr}^{-1})$	1.6E-9	1.6E-8	1.6E-7	...	3.5E-7	6.0E-7	...	*1.6E-7[a]
$\Delta M_{\mathrm{env}}/M_\odot$	3.7E-7	2.2E-7	1.4E-7	...	1.4E-7	2.2E-7	...	*1.0E-5
$\log r_{\mathrm{H}}/R_\odot$	-2.488	-2.476	-2.463	...	-2.453	-2.441	...	*-2.456
$\log T_{\mathrm{H}}(\mathrm{K})$	7.67	7.82	7.98	...	8.05	8.11	...	*8.41
$\log \rho_{\mathrm{H}}(\mathrm{g\ cm}^{-3})$	2.78	2.36	1.83	...	1.56	1.17	...	*3.22
$\log P_{\mathrm{H}}(\mathrm{dyn\ cm}^{-2})$	18.59	18.31	18.04	...	17.98	17.98	...	*19.83
$\log \epsilon_{\mathrm{n}}(\mathrm{ergs\ g}^{-1}\mathrm{s}^{-1})$	9.32	10.54	11.72	...	12.08	12.23	...	*9.34
$\log L_{\mathrm{n}}/L_\odot$	2.048	3.049	4.049	...	4.389	4.621	...	*4.049
$\log L/L_\odot$	2.072	3.073	4.077	...	4.423	4.690	...	*4.087
$\log R/R_\odot$	-2.472	-2.456	-2.421	...	-2.376	-1.746	...	*-2.334
$\log T_{\mathrm{eff}}(\mathrm{K})$	5.516	5.758	5.992	...	6.056	5.807	...	*5.950
$\log \tau_{\mathrm{g}}(\mathrm{s})$	6.86	5.94	5.64	...	stable	stable	...	...

[a] The asterisk indicates the quantities for the model whose ΔM_{env} is artificially set to be $10^{-5} M_\odot$ to mimic the "surface hydrogen burning" model.

TABLE 2
STEADY HYDROGEN BURNING MODELS ($M = 1.25 M_\odot$)

$\dot{M}(M_\odot \mathrm{yr}^{-1})$	1.0E-9	1.0E-8	1.0E-7	2.1E-7	...	4.5E-7	5.35E-7
$\Delta M_{\mathrm{env}}/M_\odot$	1.6E-6	9.3E-7	5.7E-7	5.4E-7	...	6.8E-7	1.1E-6
$\log r_{\mathrm{H}}/R_\odot$	-2.306	-2.298	-2.282	-2.273	...	-2.257	-2.250
$\log T_{\mathrm{H}}(\mathrm{K})$	7.61	7.75	7.91	7.97	...	8.03	8.06
$\log \rho_{\mathrm{H}}(\mathrm{g\ cm}^{-3})$	2.72	2.30	1.79	1.58	...	1.20	1.04
$\log P_{\mathrm{H}}(\mathrm{dyn\ cm}^{-2})$	18.46	18.19	17.89	17.82	...	17.76	17.78
$\log \epsilon_{\mathrm{n}}(\mathrm{ergs\ g}^{-1}\mathrm{s}^{-1})$	8.51	9.74	10.93	11.30	...	11.54	11.61
$\log L_{\mathrm{n}}/L_\odot$	1.845	2.845	3.845	4.167	...	4.499	4.574
$\log L/L_\odot$	1.868	2.869	3.872	4.196	...	4.538	4.628
$\log R/R_\odot$	-2.283	-2.267	-2.229	-2.194	...	-2.025	-1.511
$\log T_{\mathrm{eff}}(\mathrm{K})$	5.370	5.612	5.844	5.908	...	5.909	5.674
$\log \tau_{\mathrm{g}}(\mathrm{s})$	7.62	6.68	6.14	7.36	...	stable	stable

TABLE 3
STEADY HYDROGEN BURNING MODELS ($M = 1.0 M_\odot$)

$\dot{M}(M_\odot \mathrm{yr}^{-1})$	1.0E-9	1.0E-8	1.0E-7	1.3E-7	...	2.5E-7	3.6E-7
$\Delta M_{\mathrm{env}}/M_\odot$	8.0E-6	4.7E-6	3.2E-6	3.2E-6	...	3.9E-6	6.7E-6
$\log r_{\mathrm{H}}/R_\odot$	-2.099	-2.087	-2.059	-2.053	...	-2.034	-2.018
$\log T_{\mathrm{H}}(\mathrm{K})$	7.57	7.71	7.86	7.88	...	7.93	7.96
$\log \rho_{\mathrm{H}}(\mathrm{g\ cm}^{-3})$	2.51	2.08	1.54	1.46	...	1.20	0.97
$\log P_{\mathrm{H}}(\mathrm{dyn\ cm}^{-2})$	18.22	17.93	17.61	17.58	...	17.50	17.47
$\log \epsilon_{\mathrm{n}}(\mathrm{ergs\ g}^{-1}\mathrm{s}^{-1})$	7.82	9.04	10.20	10.32	...	10.59	10.66
$\log L_{\mathrm{n}}/L_\odot$	1.845	2.845	3.845	3.959	...	4.243	4.401
$\log L/L_\odot$	1.868	2.869	3.871	3.986	...	4.274	4.439
$\log R/R_\odot$	-2.055	-2.026	-1.946	-1.923	...	-1.792	-1.358
$\log T_{\mathrm{eff}}(\mathrm{K})$	5.256	5.492	5.702	5.720	...	5.726	5.550
$\log \tau_{\mathrm{g}}(\mathrm{s})$	8.31	7.39	7.20	8.08	...	stable	stable

Paczyński (1970). (Here the core mass corresponds to the white dwarf mass M.) The exact value of L_{RG} as a function of M depends on the opacity and abundance of the accreted matter, so that we give L_{RG} in Table 5 from our asymptotically obtained values.

As the luminosity approaches L_{RG} the radius of the white dwarf gets larger. The open and filled circles indicate thermally unstable and stable models, respectively. Models brighter than the critical luminosity, L_{stable}, around the "knee" of the model sequence are thermally stable.

Table 5 summarizes the critical luminosities L_{stable} and $\dot{M}_{\mathrm{stable}}$, and the limiting luminosities L_{RG} and corresponding $\dot{M}_{\mathrm{RG}}$. The critical $\dot{M}_{\mathrm{stable}}$ and $\dot{M}_{\mathrm{RG}}$ are, respectively, approximated by

$$\dot{M}_{\mathrm{stable}} = 3.066 \times 10^{-7} (M/M_\odot - 0.5357) M_\odot \mathrm{yr}^{-1}, \quad (5)$$

and

$$\dot{M}_{\mathrm{RG}} = 6.682 \times 10^{-7} (M/M_\odot - 0.4453) M_\odot \mathrm{yr}^{-1}. \quad (6)$$

The ratio between these two rates only slightly depends on M as $\dot{M}_{\mathrm{RG}}/\dot{M}_{\mathrm{stable}}$ = 2.3, 2.5, 2.7, and 3.0 for M = 1.38, 1.25, 1.0, and 0.7 $M_\odot$, respectively. The loci on the HR diagram and the stability of the steady-state models agree with the results of Sienkiewicz (1975, 1980). The above results have recently been confirmed by Shen & Bildsten (2007), who have applied the analytic approach with the one zone model and examined the metallicity dependence.

TABLE 4
STEADY HYDROGEN BURNING MODELS ($M = 0.8M_\odot$)

$\dot{M}(M_\odot \mathrm{yr}^{-1})$	1.0E-9	1.0E-8	7.5E-8	...	1.0E-7	2.2E-7
$\Delta M_\mathrm{env}/M_\odot$	2.0E-5	1.2E-5	1.0E-5	...	1.0E-5	2.0E-5
$\log r_\mathrm{H}/R_\odot$	-1.990	-1.973	-1.934	...	-1.925	-1.888
$\log T_\mathrm{H}$(K)	7.56	7.69	7.82	...	7.84	7.89
$\log \rho_\mathrm{H}$(g cm^{-3})	2.37	1.93	1.44	...	1.34	1.01
$\log P_\mathrm{H}$(dyn cm^{-2})	18.06	17.76	17.46	...	17.42	17.31
$\log \epsilon_\mathrm{n}$(ergs g^{-1}s^{-1})	7.45	8.65	9.64	...	9.76	10.04
$\log L_\mathrm{n}/L_\odot$	1.845	2.845	3.720	...	3.845	4.188
$\log L/L_\odot$	1.867	2.869	3.746	...	3.871	4.218
$\log R/R_\odot$	-1.921	-1.874	-1.751	...	-1.708	-1.255
$\log T_\mathrm{eff}$(K)	5.189	5.416	5.574	...	5.583	5.444
$\log \tau_\mathrm{g}$(s)	8.68	7.83	8.47	...	stable	stable

TABLE 5
STABILITY BOUNDARY FOR STEADY BURNING MODELS

	Stability Boundary			Red Giant Boundary	
$M/M_\odot$	$\dot{M}_\mathrm{stable}(M_\odot \mathrm{yr}^{-1})$	$\log L_\mathrm{stable}/L_\odot$		$\dot{M}_\mathrm{RG}(M_\odot \mathrm{yr}^{-1})$	$\log L_\mathrm{RG}/L_\odot$
0.5	1.65E-8	3.08	...	6.9E-8	3.71
0.6	3.25E-8	3.38	...	1.2E-7	3.95
0.7	5.35E-8	3.60	...	1.6E-7	4.08
0.8	7.75E-8	3.76	...	2.3E-7	4.23
0.9	1.05E-7	3.89	...	2.95E-7	4.35
1.0	1.35E-7	4.00	...	3.7E-7	4.45
1.1	1.65E-7	4.09	...	4.4E-7	4.53
1.2	1.95E-7	4.16	...	5.1E-7	4.60
1.25	2.15E-7	4.20	...	5.4E-7	4.64
1.30	2.35E-7	4.25	...	5.8E-7	4.67
1.35	2.55E-7	4.28	...	6.0E-7	4.70
1.38	2.75E-7	4.31	...	6.2E-7	4.71

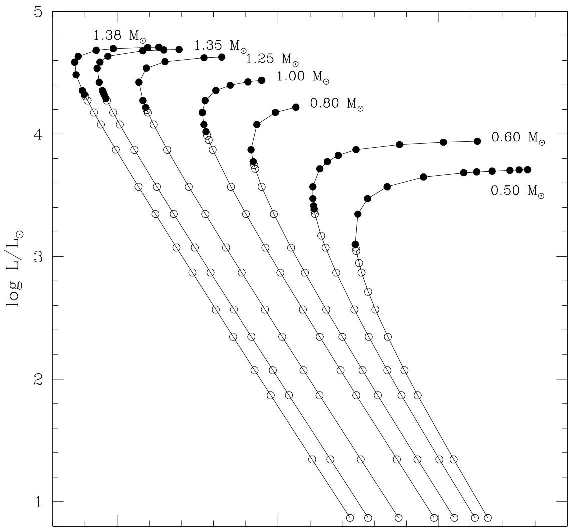

FIG. 1.— Loci of steady models in the HR diagram. Each sequence corresponds to a mass of white dwarf which accretes matter of solar composition at various rates. The accretion rate determines the luminosity because hydrogen is assumed to burn at the same rate of accretion. Open and filled circles indicate thermally unstable and stable models, respectively.

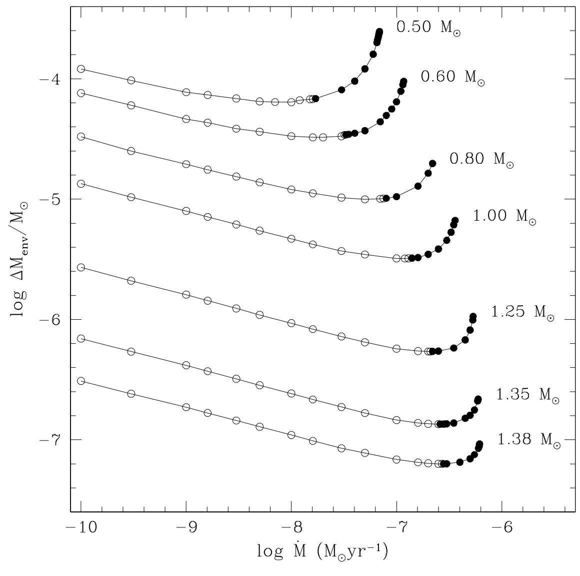

FIG. 2.— The mass of the hydrogen-rich envelope versus accretion rate for various white dwarf masses of steady models. Open and filled circles indicate thermally unstable and stable models, respectively.

Figure 2 shows the hydrogen-rich envelope mass ΔM_env as a function of $\dot{M}$ for each mass of the accreting white dwarf. The symbols have the same meanings as those in Figure 1. The larger the white dwarf mass, the smaller the envelope mass for a given accretion rate. The mass ΔM_env attains minimum at the accretion rate $\dot{M}_\mathrm{stable}$ in equation (3) corresponding to L_stable. For smaller ΔM_env, T_H would be too low to give enough L_n. For $\dot{M} > \dot{M}_\mathrm{stable}$, the models are thermally stable.

Figure 3 shows growth time (= $1/\sigma$) of the thermal insta-

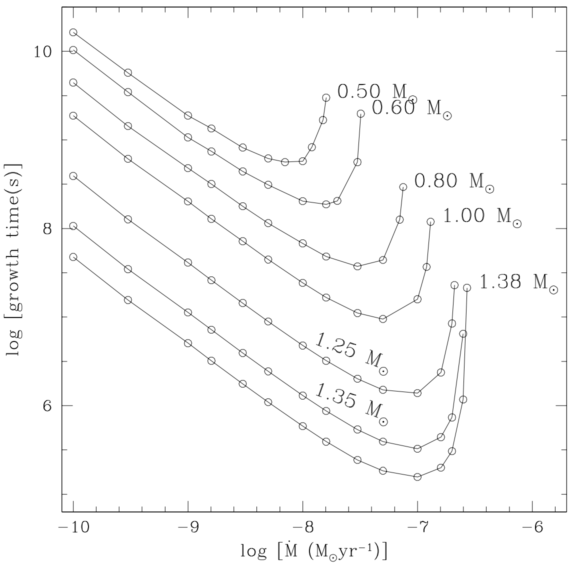

FIG. 3.— Growth time of the thermal instability of the hydrogen burning shell is plotted against the accretion rate for each white dwarf mass.

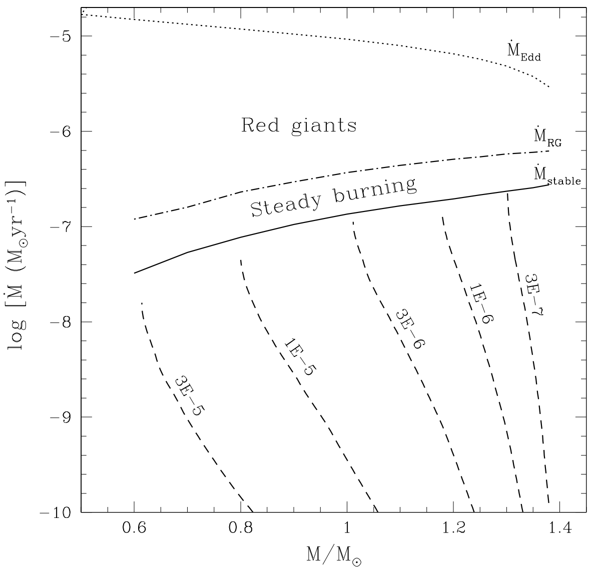

FIG. 4.— The properties of H-burning shells in accreting white dwarfs are shown in the white dwarf mass M – accretion-rate $\dot{M}$ plane. If the accretion rate is lower than the solid line of $\dot{M}_{\rm stable}$, H-burning shells are thermally unstable. A dashed line traces the locus of the envelope mass $\Delta M_{\rm env}/M_\odot$. For given M and $\dot{M}$, the envelope masses of these steady-state models are smaller than the envelope masses of the "ignition" models given in Figure 9 in Nomoto (1982) because of the higher entropy in the steady-state models than th 'ignition" models (see text for more details). In the area between the solid ($\dot{M}_{\rm stable}$) and dash-dotted ($\dot{M}_{\rm RG}$) lines, the H-burning shell burns steadily and the star is located around the "knee" or the horizontal branch on a locus of steady-state white dwarf models. Above the dash-dotted line for $\dot{M}_{\rm RG}$, the stellar envelope is expanded to a red-giant size and a strong wind occurs. Dotted line indicate the Eddington accretion rate $\dot{M}_{\rm Edd}$ as a function of M.

bility of steady-state white dwarf models as a function of the accretion rate $\dot{M}$ for each white dwarf mass M. For given M, the growth time decreases as $\dot{M}$ increases when $\dot{M}$ is relatively low. As $\dot{M}$ increases, the growth time reaches a minimum and increases rapidly toward the stability boundary. For given $\dot{M}$, the growth time is longer for smaller M.

To interpret the above results, we follow the description of basic physics of the stability of nuclear burning in a thin shell as summarized in Sugimoto & Fujimoto (1978) and Sugimoto & Miyaji (1981). If a temperature perturbation of $\delta T(M_r) > 0$ is applied to a nuclear burning shell, it leads to the positive change in specific entropy of $\delta s(M_r) > 0$ in most cases mainly because of the larger temperature sensitivity of nuclear reaction rate over radiative loss. Then $\delta s(M_r)$ induces the hydrostatic readjustment and the resultant temperature change is given as:

$$\delta \ln T = \frac{1}{c_{\rm g}^*}\delta s, \tag{7}$$

$$\frac{1}{c_{\rm g}^*} = \frac{1}{c_P} + \left(\frac{\partial \ln T}{\partial \ln P}\right)_s \frac{\delta \ln P}{\delta s}. \tag{8}$$

Here c_P and $c_{\rm g}^*$ denote the ordinary thermodynamic specific heat and the gravothermal specific heat, respectively.

If $c_{\rm g}^* > 0 (< 0)$, $\delta \ln T > 0 (< 0)$ for $\delta s > 0$ and shell burning is thermally unstable (stable). Thus the stability is determined by the hydrostatic readjustment $\delta \ln P/\delta s (< 0)$ due to expansion (for $\delta s > 0$), which depends on on the following two factors.

(1) *Geometry*: In the extremely thin shell, the pressure at the bottom of the thin envelope is determined as:

$$P = \frac{GM^2(1-q)}{4\pi R^4}, \tag{9}$$

where R is the radius of the white dwarf, and P is determined only by the column density above the radius r. Therefore, the effect of expansion for $\delta \ln P/\delta s$ is too small to cool the shell and to stabilize nuclear burning. This is the main reason for thin shell burning to be unstable, being the case for low $\dot{M}$. For high $\dot{M}$, entropy at the burning shell is larger, thus leading to a more extended envelope as seen in Figure 1. Then the effect of hydrostatic readjustment (expansion) is larger and tends to stabilize nuclear shell burning.

(2) *Equation of State*: If electrons are degenerate, P depends only weakly on T, which makes the effect of expansion too small to stabilize nuclear burning upon $\delta T > 0$. This is the case for low $\dot{M}$ and thus low s at the burning shell. On the contrary, for high $\dot{M}$ and L, especially, near their RG values, radiation pressure is important and its large T sensitivity stabilizes shell burning (see also (Shen & Bildsten 2007)).

At $L_{\rm stable} < L < L_{\rm RG}$ (or $\dot{M}_{\rm stable} < \dot{M} < \dot{M}_{\rm RG}$), therefore, these combined effects of radiation pressure and the extended envelope structure lead to stable burning. This is why $\dot{M}_{\rm stable}$ is smaller than $\dot{M}_{\rm RG}$ by only a factor of ~ 2.3 - 2.7. (See Fujimoto (1982b) for further details on the stability of the thin shell approximation models.)

Figure 4 summarizes the properties of steady-state models accreting hydrogen-rich matter. The vertical axis is the accretion rate $\dot{M}$ and the horizontal axis is the white dwarf mass M. The model properties are classified as follows:

(1) The models are thermally unstable in the area below the solid line to show $\dot{M}_{\rm stable}$. The dashed line indicates the loci where the envelope mass $\Delta M_{\rm env}$ is constant; the value attached to each dashed line indicates $\Delta M_{\rm env}/M_\odot$. These envelope masses of the steady state models tend to be smaller than those obtained by Sienkiewicz (1975) by a factor of 1.2 - 1.3, but can be regarded as being consistent in view of the

updated opacity in the present study.

(2) In the area above the solid line of $\dot{M}_{\rm stable}$, accreting white dwarfs are thermally stable so that hydrogen burns steadily in the burning shell.

(3) Above the dash-dotted line for $\dot{M}_{\rm RG}$, the accreted matter is accumulated faster than consumed into He by H-shell burning. As a result the accreted matter is piled up to form a red-giant size envelope Nomoto et al. (1979). The accretion rate is limited by the Eddington's critical accretion rate $\dot{M}_{\rm Edd}$ which is defined as

$$\dot{M}_{\rm Edd} = \frac{4\pi cR}{\kappa}. \tag{10}$$

For $\kappa = 0.2(1+X)$, $\dot{M}_{\rm Edd}$ is shown by the dotted line in Figure 4. Note that, at this critical rate, the luminosity produced by the gravitational energy release associated with accretion reaches the Eddington's critical luminosity.

This diagram is similar to Figure 9 in Nomoto (1982) except that the envelope mass in the latter is for the "ignition" models. Nomoto (1982) obtained the "ignition" model by calculating the time-dependent evolution of the mass accreting white dwarf with the Henyey code to find the stage where the nuclear energy generation rate $\epsilon_{\rm n}$ first exceeds the radiative energy loss rate at the bottom of the envelope (see (Townsley & Bildsten 2004) for the most updated "ignition" mass in one zone models). The envelope mass of the "ignition" model thus determined is larger than the envelope mass $\Delta M_{\rm env}$ of our steady-state models because of the lower entropy in the "ignition" model for given M and $\dot{M}$.

The stability of our steady-state models are consistent with the previous computations for long-term evolutions of accreting white dwarfs. For example, Sion et al. (1979) have found that a $1.2M_\odot$ white dwarf accreting at a rate $1.03 \times 10^{-7}M_\odot$ yr^{-1} gives rise to repetitive hydrogen shell flashes, while a $1.3M_\odot$ white dwarf accreting at a rate $2.71 \times 10^{-7}M_\odot$ yr^{-1} undergoes stable hydrogen burning. Paczyński & Żytkow (1978) have also shown that, for a $0.8M_\odot$ white dwarf, the stability boundary of the hydrogen burning shell is located around $\dot{M} \sim 10^{-7}M_\odot$ yr^{-1}. Consulting with Figures 2 and 4, we can confirm that those evolutionary results agree very well with our results for steady-state models.

4. DISCUSSION

4.1. *On "Surface Hydrogen Burning" Models*

Starrfield et al. (2004) wrote that their "surface hydrogen burning" models of mass accreting $1.25M_\odot$ and $1.35M_\odot$ white dwarfs are thermally stable for accretion rates ranging from $1.6 \times 10^{-9}M_\odot$ yr^{-1} to $8.0 \times 10^{-7}M_\odot$ yr^{-1}. The stability property of their models, however, differs from those of our steady-state models as well as all other models (Sienkiewicz 1980; Fujimoto 1982a; Shen & Bildsten 2007). Our models indicate that the hydrogen burning shell in the $1.35M_\odot$ model is thermally unstable if the accretion rate is less than $2.5 \times 10^{-7}M_\odot$ yr^{-1} ($2.1 \times 10^{-7}M_\odot$ yr^{-1} for $1.25M_\odot$) (Fig. 2).

Starrfield et al. (2004) also wrote that the mass accretion onto the hot white dwarf just after a nova explosion leads to a stable surface hydrogen burning. However, the time-dependent calculations by Prialnik & Kovetz (1995) indicated that the H-accretion onto the hot white dwarfs with the interior temperatures of $1-5 \times 10^7$ K leads to a shell flash for $M = 0.65-1.4\,M_\odot$.

In addition to the difference in the stability property, radii of Starrfield et al.'s models tend to be smaller than those of our models (Fig. 5 below). In particular, their highest luminosity model ($M = 1.35M_\odot$ and $\dot{M} = 8 \times 10^{-7}M_\odot$ yr^{-1}) has a white-dwarf size, while our results indicate that such a high accretion rate makes the star of a red-giant size (Fig. 4).

These discrepancies are caused by the extremely coarse zoning adopted in Starrfield et al.'s computations. Starrfield et al. (2004) adopted a surface zone mass of $10^{-5}M_\odot$, which is much larger than the entire envelope mass of the steady-state models of $M = 1.35M_\odot$ and $1.25M_\odot$ as seen in Figures 2 and 4. This means that the envelope of the "surface hydrogen burning" model is approximated by a single zone having a single temperature and density. Furthermore, the "surface zone" is much deeper than the realistic hydrogen-rich envelope of the steady-state model corresponding to the same white dwarf mass and the accretion rate.

Table 1 compares the two white dwarf models with $M = 1.35M_\odot$ accreting hydrogen-rich matter at a rate of $\dot{M} = 1.6 \times 10^{-7}M_\odot$ yr^{-1}. The steady-state model calculated in the present study has $\Delta M_{\rm env} = 1.4 \times 10^{-7}M_\odot$ and $\log T_{\rm H}({\rm K}) = 7.98$ (4th column). For the model with the asterisk (7th column), the mass of the hydrogen-rich envelope is artificially set to be $\Delta M_{\rm env} = 10^{-5}M_\odot$, which is the same as the "surface zone mass" adopted by Starrfield et al. (2004). According to equation (9) and $T_{\rm H}^4 \propto P_{\rm H} \propto \Delta M_{\rm env}$, the temperature at the burning shell ($\log T_{\rm H}({\rm K}) = 8.41$) is much higher than those of the steady-state model.

Such a high temperature is comparable to that of the surface zone of Starrfield et al. (2004), from which we see the reason why Starrfield et al. (2004) obtain very high temperature at the "surface zone". They treated the envelope between the region of $\log(1-q) \sim (-5)-(-22)$ by a single mass zone, while our steady-state models resolve the H-rich envelope with ~ 50 mass zones. Obviously, the zoning adopted by Starrfield et al. (2004) is too coarse to obtain a physically realistic stellar model.

In the heavy envelope model, the temperature at the hydrogen burning shell is so high that all accreted hydrogen burns in one typical time step to compute mass accretion, as Starrfield et al. (2004) states "it takes less time than the time step ($\sim 2 \times 10^6$ s) for all the infalling hydrogen to burn to helium in this zone". In this case, the nuclear energy generation rate $\epsilon_{\rm n}$ is determined not by the temperature-dependent nuclear reaction rate but by the supplying rate of nuclear fuel as

$$\epsilon_{\rm n} = \frac{XQ\dot{M}}{\Delta M_{\rm env}}. \tag{11}$$

Despite such a high temperature as $\log T({\rm K}) = 8.41$, the energy generation rate thus determined is $\epsilon_{\rm n} = 2.2 \times 10^9$ ergs g^{-1} s^{-1}, which is much lower than the β–limited reaction rate of the hot CNO cycle $\epsilon_\beta = 6 \times 10^{13}(X_{\rm CNO}/0.01)$ ergs g^{-1} s^{-1}. Because $XQ\dot{M}/\Delta M_{\rm env}$ is constant, being independent of the temperature, the nuclear burning is stable; it is also steady as expressed by equation (1). In other words, the assumed envelope mass $\Delta M_{\rm env}$ is too large and hence the temperature at the nuclear burning shell is too high for the mass accretion rates they assumed. All the accreted hydrogen-rich matter should have been consumed long before it is pushed into a layer as deep as $M - M_r \sim 10^{-5}M_\odot$ (Nariai et al. 1980).

4.2. *Comparisons with Supersoft X-ray Sources*

Supersoft X-ray sources are suggested to be accreting white dwarfs in which steady hydrogen burning is taking place (e.g.,

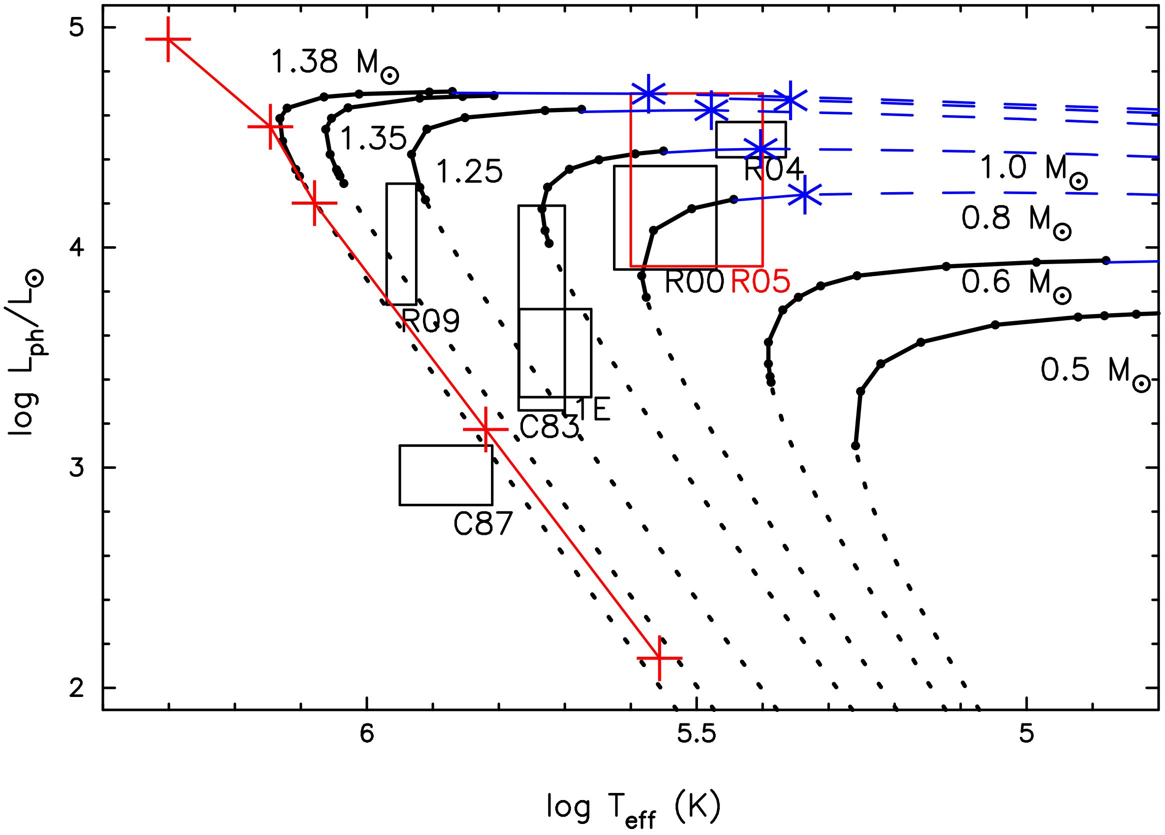

FIG. 5.— Loci of steady-state models in the HR diagram together with Starrfield et al.'s (2004) results and positions of several supersoft X-ray sources. The filled small circles on the solid line are the same solutions as in Figure 1. The white dwarf mass is attached to each curve. The solid line-parts indicate the stable steady-state solution, while the dotted line parts correspond to the unstable solutions as shown in Figure 1. In the dashed line parts, the optically thick winds are predicted to blow (Kato & Hachisu 1994), so that supersoft X-rays could be absorbed by the wind matter and not be detected. The solid line with the crosses show the positions of the "surface hydrogen burning" models (1.35 $M_{\odot}$) (Starrfield et al. 2004). Positions of several supersoft X-ray sources are plotted by squares (taken from Figure 1 of Starrfield et al. 2004), i.e., R09 (RX J0925.7–4758), C87 (CAL87), C83 (CAL83), 1E (1E0035.4–7230), R00 (RX J0019.8+2156), R04 (RX J0439.8–6809). In addition, the position of the supersoft X-ray source RX J0513.9–6951 (R05) is also plotted.

van den Heuvel et al. 1992). Starrfield et al. (2004) argued that the properties of their "surface hydrogen burning" models agree with some of supersoft X-ray sources. In this subsection, therefore, we compare our steady burning models and the "surface hydrogen burning" models in the HR diagram with several observed supersoft X-ray sources.

In the HR diagram of Figure 5, we show the loci of the steady burning models for given M. The filled small circles on the solid lines indicate the thermally stable models in Figure 1, while the dotted lines correspond to the unstable solutions. For comparison, the "surface hydrogen burning" models with $M = 1.35 M_{\odot}$ (Starrfield et al. 2004) are shown by the crosses. In contrast to the "surface hydrogen burning" models, the sequences of stable models shown by the solid lines bends rightward because of the increasing radius with increasing $\dot{M}$.

The large boxes in Figure 5 indicate the positions of several supersoft X-ray sources taken from Starrfield et al. (2004). The bolometric luminosities of supersoft X-ray sources are very uncertain because very soft X-rays are easily absorbed by neutral hydrogen. For example, although the luminosity of CAL 87 in LMC is lower than the $1.38 M_{\odot}$ white dwarf sequence in Figure 5, the bolometric luminosity of CAL 87 has been estimated to be a few times 10^{37}ergs s^{-1}, far above the error box (Greiner 2000; Greiner et al. 2004). Taking into account such large uncertainties in the bolometric luminosity, we may consider that the loci of luminous supersoft X-ray sources in the HR diagram are not inconsistent with the loci of thermally stable models (solid line parts). We suggest that no supersoft X-ray source is expected in the dashed line region, because optically thick winds are predicted to blow in this region (Kato & Hachisu 1994; Kato 1996) and the matter in the winds would absorb most of the supersoft X-rays.

We have added one more supersoft X-ray source in the LMC, RX J0513.9–6951. Schaeidt, Hasinger, & Trümper (1993) estimated the surface temperature $T_{\rm ph} \sim 30-40$ eV and the total luminosity $L_{\rm ph} \sim L_{\rm x} \sim 2 \times 10^{38}$ ergs s^{-1} by a black-body fitting. On the other hand, Gänsicke et al. (1998) obtained $L_{\rm ph} \sim L_{\rm x} \sim (3-9) \times 10^{37}$ ergs s^{-1} by their model atmosphere of the white dwarf. This is a quasi-regular transient X-ray source with a relatively short X-ray-on (~ 40 days) and a long X-ray-off (~ 100 days) states. Hachisu & Kato (2003a) proposed a transition model, in which the white dwarf expands or contracts intermittently. In this model, an optically thick wind occurs only when the star is expanded, and the X-ray-off state is interpreted as this expanded phase where the supersoft X-rays are absorbed by the wind materials.

The existence of such a transient supersoft X-ray source as shown in Figure 5 may support our results that there exist envelope expansions for high mass accretion rates. Note that in Starrfield et al.'s models the envelopes do not expand even for higher mass accretion rates. This transient X-ray phenomenon is common at least in the LMC and our Galaxy, because such a system exists not only in the LMC (in a lower metallicity environment) but also in our Galaxy. A Galactic supersoft X-ray source, V Sge, which is not shown in Figure 5, is a sister system to RX J 0513.9-6951 (e.g., Greiner & van Teeseling

1998; Hachisu & Kato 2003b).

The above comparison shows that the properties of luminous supersoft X-ray sources are consistent with our steady hydrogen-burning white dwarf models.

5. CONCLUDING REMARKS

We have reinvestigated the properties of accreting white dwarfs by constructing steady-state models, in which hydrogen shell burning consumes hydrogen at the same rate as the white dwarf accretes it. We have confirmed that these steady models are stable only when the accretion rate is higher than $\dot{M}_{\rm stable}$ in equation (3).

Our results contradict the "surface hydrogen burning" models by Starrfield et al. (2004) who found quiescent stable hydrogen burning for a wide range of accretion rates down to $\dot{M} \sim 10^{-9} M_\odot$ yr^{-1}. We believe we have shown that quiescence of "surface hydrogen burning" results from the too large zone mass ($\sim 10^{-5} M_\odot$) in the outer part of the numerical models, and that hydrogen burning must occur in a much more superficial layer ($\sim 10^{-7} M_\odot$).

We have shown that the positions on the HR diagram of most of the luminous supersoft X-ray sources are consistent with the white dwarfs accreting matter at rates high enough for hydrogen shell burning to be thermally stable.

The narrow range of the accretion rate that leads to the steady and stable hydrogen burning has been confirmed. Despite that property, how the progenitor white dwarfs for SNe Ia could grow their masses to the Chandrasekhar mass by accreting hydrogen-rich matter has been discussed in Hachisu et al. (e.g., 1996); Li & van den Heuvel (e.g., 1997); Hachisu et al. (e.g., 1999a,b); Langer et al. (e.g., 2000); Han & Podsiadlowski (e.g., 2004); Nomoto et al. (e.g., 2000, 2005)

This work has been supported in part by the grant-in-Aid for Scientific Research (14047206, 14540223, 16540211, 16540219, 17030005, 17033002, 18104003, 18540231) from the JSPS and MEXT in Japan.

REFERENCES

Caughlan, G.R., & Fowler, W.A. 1988, Atomic Data and Nuclear Data Tables 40, 283
Fujimoto, M.Y. 1982, ApJ, 257, 752
Fujimoto, M.Y. 1982, ApJ, 257, 767
Graboske, H.C., DeWitt, H.E., Grossman, A.S., & Cooper, M.S. 1973, ApJ, 181, 457
Gänsicke, B. T., van Teeseling, A., Beuermann, K., & de Martino, D. 1998, A&A, 333, 163
Greiner, J., & van Teeseling, A., 1998, A&A, 339, L21
Greiner, J., 2000, New Astr, 5, 137
Greiner J., Iyudin A., Jimenez-Garate M., Burwitz V., Schwarz R., DiStefano R., Schulz N., 2004, in IAU Coll. 194, Compact Binaries in the Galaxy and Beyond, eds. G. Tovmassian, E. Sion, Rev Mex AA, 20, 18
Hachisu, I., & Kato, M. 2001, ApJ, 558, 323
Hachisu, I., & Kato, M. 2003a, ApJ, 590, 445
Hachisu, I., & Kato, M. 2003b, ApJ, 598, 527
Hachisu, I., & Kato, M. 2006, ApJ, 642, L53
Hachisu, I., Kato, M., & Nomoto,K. 1996, ApJ, 470, L97
Hachisu, I., Kato, M., Nomoto, K., & Umeda, H. 1999a, ApJ, 519,314
Hachisu, I., Kato, M., & Nomoto,K. 1999b, ApJ, 522, 487
Han, Z., & Podsiadlowski, Ph. 2004, MNRAS, 350, 1301
Hillebrandt, W., & Niemeyer, J. 2000, ARA&A, 38, 191 (Errata at http://arjournals.annualreviews.org/doi/abs/10.1146/annurev.aa.38.010100.200001)
Iben, I., Jr. 1982, ApJ, 259, 244
Iglesias, C.A., & Rogers, F.J. 1996, ApJ, 464, 943
Kato, M. & Hachisu, M. 1994, ApJ, 437, 802
Kato, M. 1996, in Supersoft X-ray Sources, ed. J. Greiner (Heidelberg: Springer), 15
Kawai, S., Saio, H., & Nomoto, K. 1987, ApJ, 315, 229
Langer, N., Deutschmann, A., Wellstein, S., & Höflich, P. 2000, A&A, 362, 1046
Li, X.-D., & van den Heuvel, E.P.J, 1997, ApJ, 322, L9
Livio, M. 2000, in Type Ia Supernovae: Theory and Cosmology, eds. J. Truran & J. Niemeyer (Cambridge: Cambridge Univ. Press), 33
Nariai, K., Nomoto, K., & Sugimoto, D. 1980, PASJ, 32, 473
Nomoto, K. 1982, ApJ, 253, 798
Nomoto, K., Iwamoto, K., & Kishimoto, N. 1997, Science, 276, 1378
Nomoto, K., Nariai, K., & Sugimoto, D. 1979, PASJ, 31, 287
Nomoto, K., Thielemann, F.-K., & Yokoi, K. 1984, ApJ, 286, 644
Nomoto, K., Umeda, H., Kobayashi, C., Hachisu, I., Kato, M., & Tsujimoto, T. 2000, in Type Ia Supernovae: Theory and Cosmology, eds. J. Truran & J. Niemeyer (Cambridge: Cambridge Univ. Press), 63 (astro-ph/0003134)
Nomoto, K., Uenishi, T., Kobayashi, C., Umeda, H., Ohkubo, T., Hachisu, I., & Kato, M. 2003, in From Twilight to Highlight: The Physics of Supernovae, eds. W. Hillebrandt & B. Leibundgut, ESO-Springer Ser. "ESO Astrophysics Symposia" (Berlin: Springer-Verlag), 115 (astro-ph/0308138)
Nomoto, K., Suzuki, T., Deng, J., Uenishi, T., & Hachisu, I. 2005, in 1604-2004: Supernovae as Cosmological Lighthouses, ASP Conf. Ser. 342, eds. M. Turatto, et al. (San Francisco: ASP), 105 (astro-ph/0603432)
Paczyński, B. 1970, Acta Astr., 20, 47
Paczyński, B. 1983, ApJ, 264, 282
Paczyński, B., & Żytkow, A.N. 1978, ApJ, 222, 604
Prialnik, D. 1986, ApJ, 310, 222
Prialnik, D., & Kovetz, A. 1995, ApJ, 445, 789
Schaeidt, S., Hasinger, G., & Trümper, J., 1993, A&A, 270, L9
Schwarzschild, M. & Härm, R. 1965, ApJ, 142, 855
Shen, K.J., & Bildsten, L. 2007, ApJ, in press (astro-ph/0702049)
Sienkiewicz, R. 1975, A&A, 45, 411
Sienkiewicz, R. 1980, A&A, 85, 295
Sion, E.M., Acierno, M.J., & Tomczyk, S. 1979, ApJ, 230, 832
Starrfield, S., Timmes, F.X., Hix, W.R., Sion, E.M., Sparks, W.M., & Dwyer, S.J., 2004, ApJ, 612, L53
Sugimoto, D., & Fujimoto, M. Y. 1978, PASJ, 30, 467
Sugimoto, D., & Miyaji, S. 1981, in IAU Symposium 93, Fundamental Problems in Stellar Evolution, ed. D. Sugimoto, D.Q. Lamb, & D.N. Schramm (Dordrecht: Reidel), 191
Townsley, D. M., & Bildsten, L. 2004, ApJ, 600, 390
van den Heuvel, E. P. J., Bhattacharya, D., Nomoto, K., & Rappaport, S. 1992, A&A, 262, 97
Yaron, O., Prialnik, D., Shara, M. M., & Kovetz, A. 2005, ApJ, 623, 398